# Dynamical constraints on the extreme low values of the potential vorticity in the ocean

L. N. Thomas

Woods Hole Oceanographic Institution, Woods Hole, Massachusetts, USA.

**Abstract.** High-resolution two and three-dimensional numerical experiments are used to study the manner in which advection of potential vorticity (PV) by frontal instabilities growing out of an initially symmetrically unstable flow or forced by destabilizing wind-forcing constrains the extreme minima in the PV to values near zero. The instabilities act as a PV pump, upwelling high PV water from the pycnocline while subducting low PV surface water. The positive correlation between the velocity and PV fields results in an upward eddy PV flux. When the baroclinic flow is forced by down-front winds, which exert an upward, PV-reducing, frictional PV flux, the eddy and surface frictional PV fluxes were found to scale with one another. This PV pump mechanism tends to increase PV in the surface boundary layer and constrains the extreme low values of the PV from dropping below zero at the expense of reducing the PV in the pycnocline. When the wind alternates orientation between down-front and up-front orientations, PV is both removed from and injected into the fluid. The PV pump mechanism limits the reduction of PV by down-front winds but not the enhancement of PV by up-front winds, causing the skewness of the isopycnal PV distribution to become positive.

## Introduction

The potential vorticity (PV) is a tracer of critical importance for balanced motions in the ocean. Under certain conditions, knowledge of the global distribution of this one tracer field, combined with information on the lateral structure of the density on horizontal surfaces is all the information that is needed to determine all dynamically important variables (e.g. the balanced flow field, density, and vertical circulation) via an inversion of elliptical equations [*Hoskins et al.*, 1985]. For adiabatic, inviscid flow, the PV is conserved so that changes in the PV field are due solely to advection. PV conservation combined with invertibility makes the equations governing the balanced flow first order in time [*McWilliams et al.*, 1998]. Consequently, if the value of the PV on each fluid parcel is known at some time (plus the surface density field), for all subsequent times all dynamical variables can be calculated. The question arises as to what sets the initial value of the PV of the fluid and whether there are any constraints on the extreme low and high values that the PV can take. The value of the PV on a fluid parcel is ultimately determined by frictional forces and or diabatic processes, since these are the only processes that can result in a Lagrangian change of PV. In this article, using numerical simulations and theoretical considerations I will illustrate the way in which wind-driven frictional forces can destroy or create PV and how hydrodynamic instabilities provide a mechanism to limit the extreme low PV values that the fluid can attain.

## Potential vorticity and hydrodynamic instability

When the Ertel PV

$$q = (f\hat{k} + \nabla \times \mathbf{u}) \cdot \nabla b, \tag{1}$$

where $f$ is the Coriolis parameter, $\mathbf{u}$ is the velocity, and $b = -g\rho/\rho_o$ is the buoyancy ($g$ is the acceleration due to gravity and $\rho$ is the density), takes the opposite sign of the Coriolis parameter, i.e. $fq < 0$, the fluid is unstable to overturning instabilities [*Hoskins*, 1974]. The instabilities that arise take different names depending on whether the vertical vorticity, stratification, or baroclinicity of the fluid is responsible for the low PV. For flows where $f\zeta_{abs}N^2 < 0$ ($\zeta_{abs} = f - u_y + v_x$) and $N^2 > 0$ the instabilities that arise are termed inertial or centrifugal. Gravitational instability occurs when $N^2 < 0$. In strongly baroclinic flows, the PV can take the opposite sign of $f$ even if $f\zeta_{abs}N^2 > 0$. This is illustrated by decomposing the PV into two terms

$$q = q_{vert} + q_{bc}, \tag{2}$$

one associated with the vertical component of the absolute vorticity and the stratification

$$q_{vert} = \zeta_{abs} N^2, \tag{3}$$

the other attributable to the horizonal components of vorticity and buoyancy gradient[1]

$$q_{bc} = \frac{\partial u}{\partial z}\frac{\partial b}{\partial y} - \frac{\partial v}{\partial z}\frac{\partial b}{\partial x}. \tag{4}$$

For a geostrophic flow, it can be shown using the thermal wind relation that (4) reduces to

$$q^g_{bc} = -f\left|\frac{\partial \mathbf{u}_g}{\partial z}\right|^2 = -\frac{1}{f}|\nabla_h b|^2, \tag{5}$$

so that $fq^g_{bc}$ is a negative definite quantity, indicating that the baroclinicity of the fluid always reduces the PV. When $|fq_{bc}| > fq_{vert}$ the instabilites that develop are termed symmetric.

Numerical experiments of flows with $fq < 0$ have shed light into the way in which overturning instabilities modify the PV field. In one such experiment, an inertially unstable equatorial flow was shown to develop inertial instabilities that through meridional advection of PV tended to homogenize PV, driving the PV to values near zero [*Hua et al.*, 1997]. In addition to mixing PV, meridional stirring by inertial instability has been proposed as a potentially important mechanism for lateral mixing of tracers near the equator [*Richards and Edwards*, 2003]. While inertial instability mixes PV horizontally, symmetric instability (SI) tends to stir PV along isopycnal surfaces which, in the strongly baroclinic regions where SI is prevalent, are slanted. Numerical experiments reveal that in its finite amplitude state, SI mixes away low PV anomalies via down-gradient advective PV fluxes [*Thorpe and Rotunno*, 1989]. The experiments mentioned above emphasize how, by mixing low and high PV fluid, overturning instabilities tend to limit the extreme low value of the PV to near zero. These experiments were not forced by boundary stresses or buoyancy fluxes, however. In this article, I will explore whether or not instabilities at wind-forced, strongly baroclinic fronts are similarly capable of limiting the extreme values of the PV. Wind forcing further complicates the matter because it can introduce frictional sinks and sources of PV that can compete with or augment the increase in PV by instabilities. The interplay between instabilities and frictional PV sources/sinks will be studied numerically, but before this, a brief description on how friction changes the PV is necessary.

[1]Note that only hydrostatic motions are being considered, so that in (4) terms in the horizontal vorticity involving lateral derivatives of the vertical velocity can be neglected.

## Frictional change of potential vorticity

Changes in the PV arise from convergences/divergences of the PV flux $\mathbf{J}$, i.e.

$$\frac{\partial q}{\partial t} = -\nabla\cdot\mathbf{J} = -\nabla\cdot\left(\mathbf{u}q + \mathbf{J}^F + \mathbf{J}^{\mathcal{D}}\right), \tag{6}$$

where $\mathbf{J}$ has advective, frictional

$$\mathbf{J}^F = \nabla b \times \mathbf{F} \tag{7}$$

($\mathbf{F}$ is a frictional or nonconservative body force) and diabatic

$$\mathbf{J}^{\mathcal{D}} = -\mathcal{D}(f\hat{k} + \nabla\times\mathbf{u}) \tag{8}$$

(where $\mathcal{D} = Db/Dt$ represents all diabatic processes, $D/Dt$ is the Lagrangian rate of change) components [*Marshall and Nurser*, 1992]. *Thomas* [2005] showed that friction acting at the sea surface will result in a reduction of the PV when

$$fJ^F_z = f\nabla_h b \times \mathbf{F}\cdot\hat{k}\Big|_{z=0} > 0. \tag{9}$$

Friction can either input or extract PV from the fluid, depending on the orientation of the frictional force and the lateral buoyancy gradient. Down-front winds (i.e. oriented in the direction of the baroclinic shear) drive PV fluxes that meet condition (9). For these winds and when the Ekman depth is shallower than the mixed layer depth, Ekman flow advects denser water over light, and convection ensues that mixes the stratification and reduces the PV. Friction injects PV into the fluid when a baroclinic current is forced by upfront winds or during frictional spin-down since the Ekman flow in both cases advects lighter water over dense and restratifies the fluid [*Boccaletti et al.*, 2007; *Thomas and Ferrari*, 2007].

## Two-dimensional baroclinic zone experiments

In this section, two dimensional numerical experiments will be utilized to illustrate mixing of PV by unforced and wind-forced SI. The initial condition used in the simulations is the baroclinic zone configuration described in *Thomas* [2005]. The configuration consists of a buoyancy field with a spatially uniform north-south gradient, $\partial b/\partial y = -S^2$, and a vertically-sheared, laterally-homogeneous, zonal geostrophic flow, $\partial u/\partial z = S^2/f$. The stratification takes a constant value $N^2_{ml}$ in a surface layer of thickness $H$. Beneath this layer the stratification increases linearly with depth so as to mimic a pycnocline. Within the surface layer, the PV, $q_{ml} = fN^2_{ml} - S^4/f$, is less than zero ($fq_ml < 0$) owing to the baroclinicity of the fluid (i.e. $N^2_{ml} > 0$),

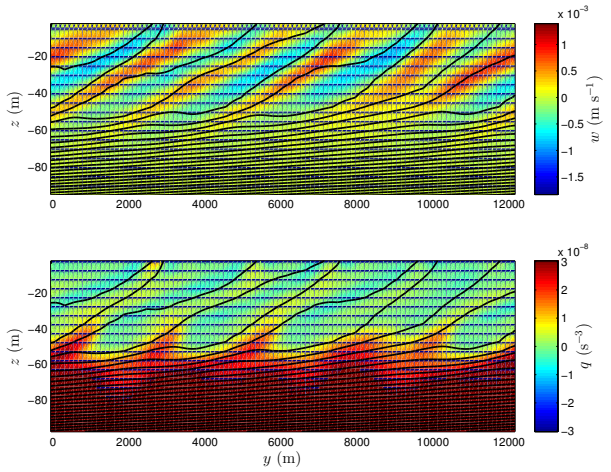


**Figure 1.** Isopycnals (black contours), vertical velocity (top), and PV (bottom) at $t = 2.0$ inertial periods from the 2D baroclinic zone experiment not forced by winds.

making the fluid susceptible to SI. Experiments with and without wind forcing were performed using the ROMS model [*Shchepetkin and McWilliams*, 2004]. In the wind-forced experiments, the wind-stress was spatially uniform, oriented in the down-front direction, of magnitude $\tau_o$, and turned on impulsively at $t = 0$, then held constant through the experiment. Boundary conditions for the flow and density fields that deviate from the initial conditions are periodic on the northern and southern edges of the model domain.

A snapshot of the vertical velocity and PV fields for the unforced experiment ($N^2_{ml} = 3.6 \times 10^{-5}$ s$^{-2}$, $S^2 = 6.3 \times 10^{-7}$ s$^{-2}$, $f = 1 \times 10^{-4}$ s$^{-1}$, $H = 38$ m) is shown in Figure 1. Overturning motions associated with SI are evident in the vertical velocity field. The overturns are slantwise, nominally aligned along isopycnal surfaces. A comparison of both fields in the figure shows that the vertical circulation downwells low PV from the surface while upwelling high PV from the pycnocline, resulting in an upward advective PV flux. The vertical advective PV flux is quantified by calculating the covariance of $w$ and $q$, $\overline{wq}$ (the overline denotes a lateral average), and is shown in Figure 2. This PV flux is largest at the base of the surface layer, peaking near the onset of the instability (at $t \approx 2$ inertial periods) and subsequently decreasing with time. This vertical exchange of PV drives the laterally averaged PV, $\overline{q}$, in the surface layer to positive values, while decreasing the PV in the pycnocline.

An experiment with the same flow parameters but forced with a down-front wind-stress of magnitude $\tau_o = 0.1$ N m$^{-2}$ was performed to investigate if the advective input of PV by SI into the surface layer can compete

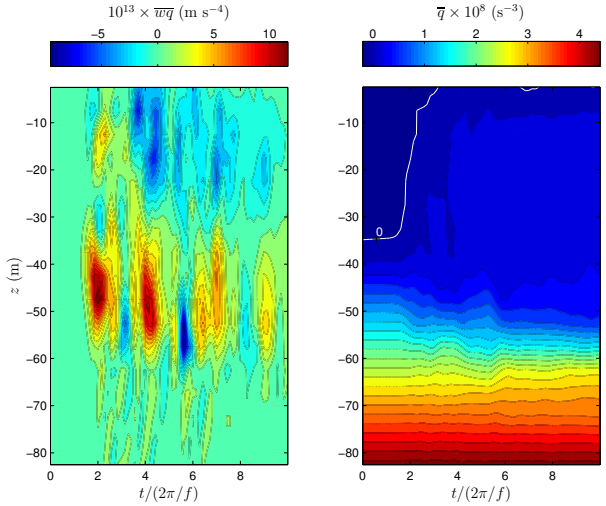


**Figure 2.** Temporal and vertical structure of the vertical advective PV flux $\overline{wq}$ (left) and the laterally averaged PV $\overline{q}$ (right) for the unforced, 2D experiment. The zero PV contour is denoted in white.

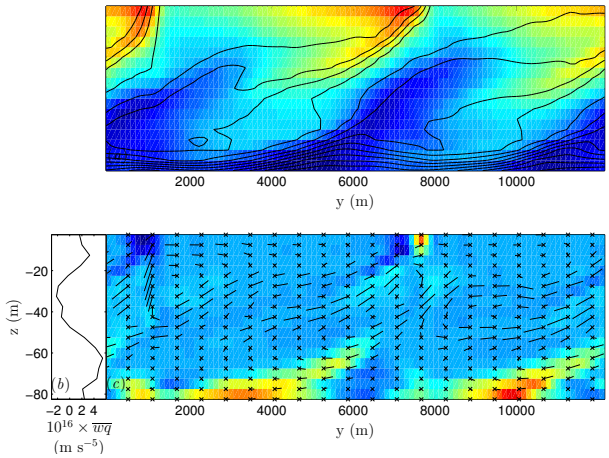


**Figure 3.** Solutions from the baroclinic zone experiment forced with a $\tau_o = 0.1$ N m$^{-2}$ wind-stress at $t = 6$ inertial periods. The zonal velocity (shades) and density (contours) fields (top); the meridionally-averaged advective PV flux (bottom left); and PV (shades) and secondary circulation (vectors) (bottom right). Warm (cool) shades indicate higher (lower) values.

with the removal of PV by friction. As in the unforced run, slantwise circulations form (Figure 3). Convergent flow associated with the vertical circulation is frontogenetic, resulting in the formation of multiple fronts with sharp frontal jets. The overturning motions induce an upward advective PV flux at the base of the surface layer, as in the unforced experiment, but with a stronger magnitude (Figure 4). A comparison between

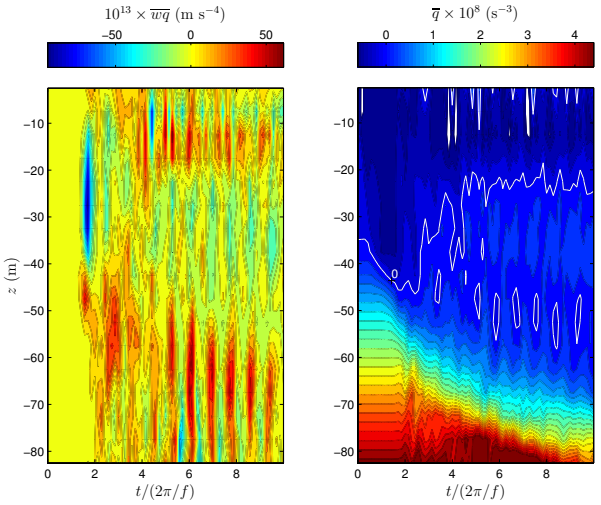


**Figure 4.** Temporal and vertical structure of the vertical advective PV flux $\overline{wq}$ (left) and the laterally-averaged PV $\overline{q}$ (right) for the wind-forced run with $\tau_o = 0.1$ N m$^{-2}$. The zero PV contour is denoted in white.

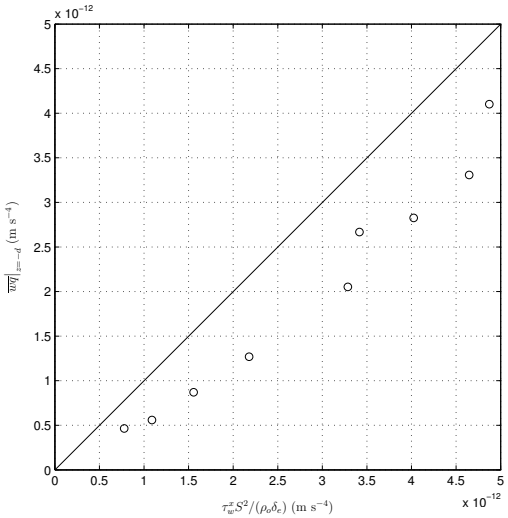


**Figure 5.** The vertical advective PV versus the scaling for the frictional PV flux for all the wind-force, 2D experiments. A line with a slope of one is plotted for reference.

Figures 2 and 4, shows that the maximum PV flux is about five times stronger in the forced experiment and that the PV flux persists in time. The persistence in $\overline{wq}$ results in a continual deepening of the surface layer, as seen in the laterally-averaged PV field. Outside of the Ekman layer (beneath $\sim 20$ m), $\overline{q}$ remains positive, suggesting that the advective PV flux associated with the forced SI is strong enough to prevent friction from reducing the PV in the surface layer below zero.

To investigate how the advective PV flux compares with the surface frictional PV flux, a series of experiments were performed where the appropriate scaling for $J_z^F$

$$[J_z^F] = \frac{\tau_o}{\rho_o \delta_e} S^2 \tag{10}$$

(where $\delta_e = 0.4\sqrt{\tau_o/\rho_o}/f$ is the Ekman layer depth) was varied and the advective PV flux was calculated. The advective PV flux measured at the base of the surface layer (at the depth $d$) is plotted against the scaling for the frictional PV flux in Figure 5. As seen in the figure, the advective and frictional PV fluxes scale nearly linearly with one another. The impact of this result can be measured in terms of a PV budget of the surface layer. The budget is constructed by taking the volume integral of (6) over the depth of the surface layer

$$\begin{aligned} \iint_{z=-d}^{z=0} \frac{\partial q}{\partial t} \mathrm{d}z\mathrm{d}y &= -\iint_{z=-d}^{z=0} \nabla \cdot \mathbf{J} \mathrm{d}z\mathrm{d}y \\ &= -\int J_z^F \mathrm{d}y\Big|_{z=0} + \int wq \mathrm{d}y\Big|_{z=-d}, \end{aligned} \tag{11}$$

where Gauss's theorem has been exploited and the periodic and no normal flow boundary conditions (on the lateral and top boundaries, respectively) have been used. The correspondence between the advective and frictional PV fluxes seen in Figure 5 implies that the two terms on the left hand side of (12) tend to cancel and hence minimize the rate of change of $\overline{q}$ in the surface layer. In this way, the vertical circulation associated with forced SI acts as a PV pump, drawing PV from the pycnocline to limit the frictional reduction of PV in the surface layer.

Although the baroclinic zone experiments described above yield insights into the dynamics of forced SI, they are admittedly limited in their two-dimensional configuration. It remains to be shown that at a fully three-dimensional front forced by winds that the PV pump mechanism described above is active. The three-dimensional numerical experiments of a wind-forced front described in the next section are designed to address this issue.

## Three-dimensional experiments of a wind-forced front

The initial conditions for the three-dimensional experiments are shown in Figure 6 and are the same as those used in *Thomas* [2007], consisting of two isolated fronts with equal and opposite lateral density gradients and frontal jets. The widths, depths, and cross-front density gradients of these fronts, and the stratification in the pycnocline are modeled after the subpolar front

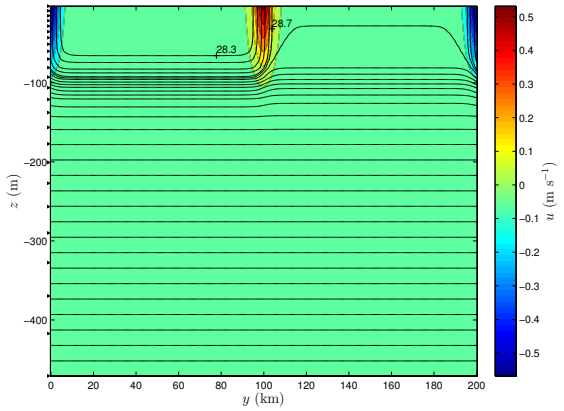


**Figure 6.** Initial conditions for the zonal velocity (shades) and density (contours) of the three-dimensional numerical experiment. The contour interval for the density is 0.1 kg m$^{-3}$. The vertical grid spacing is indicated on the left axis.

of the Japan/East Sea during the winter, which is a relatively shallow and strong front [*Thomas and Lee*, 2005]. The simulations were again run with the ROMS model, in a fully three-dimensional domain of width 45 km and 200 km in the zonal and meridional directions, respectively, and 500 m deep. The horizontal resolution was 1 km and 0.5 km in the $x$ and $y$ directions. As can be seen in the spacing of the vertical grid in Figure 6, the vertical resolution was enhanced near the surface so as to resolve the Ekman layer. Lateral boundary conditions were periodic. Two experiments were performed with different wind-forcing. In the first experiment, a spatially uniform zonal wind-stress of magnitude $\tau_w^x = \tau_o = 0.2$ N m$^2$ was turned on at the start of the experiment and left on for the duration of the experiment[2]. In the second experiment, the wind-stress was again spatially uniform, but the wind-vector rotated with time following the form

$$(\tau_w^x, \tau_w^y) = \tau_o \left(\cos(2\pi t/T), \sin(2\pi t/T)\right), \qquad (12)$$

where $\tau_o = 0.2$ N m$^2$ and $T = 3$ days. A rotating wind-stress with a period of three days was chosen to mimic the passage of storms over the fronts. The motivation for using a wind-stress of this form that removes as well as injects PV was to see if there are limitations on either the extreme low or high values of the PV that is generated when both a PV source and sink is present.

In the experiment with the constant zonal wind-stress, southward Ekman transport advects the surface density field. For the first few inertial periods ($f = 1 \times 10^{-4}$ s$^{-1}$), the flow is two-dimensional, but after $\sim 2.5$ inertial periods, the front with the eastward flow becomes unstable to three-dimensional instabilities. In contrast, the front with the westward flow remains two-dimensional throughout the experiment. At this front, the eastward wind-stress results in the formation of a stratified layer in the upper 30 m. This restratification is a consequence of the frictional injection of PV by the upfront wind-stress.

At the front with the eastward jet, the downfront wind forcing leads to the formation of low PV water, as can be seen in the maps of the PV on an isopycnal surface that outcrops at the front (Figure 7). As the front forms meanders, the frontal vertical circulation upwells water with high PV from the pycnocline and subducts low PV surface water. The positive correlation between the flow and PV anomalies implies that there is an upward along-isopycnal eddy PV flux in the same direction as the frictional PV flux. This suggests that, similar to results from the two-dimensional baroclinic zone experiments, there is a relationship between eddy and frictional PV fluxes. To quantify this relationship, the net eddy PV flux along an isopycnal layer

$$\mathscr{J}_y^e = \int \int_{z=z_b}^{z=z_t} q'' v'' \mathrm{d}z\mathrm{d}x \qquad (13)$$

where $z_t, z_b$ are the top and bottom depths of the isopycnal layer, the zonal integral is performed over the full domain, and the double primes denote the deviation from the thickness weighted isopycnal mean, i.e. $v'' = v - \overline{vh}^x / \overline{h}^x$, $h = z_t - z_b$ (the overline denotes a $x$ average) was calculated and compared to the net frictional PV flux going through the outcrop area $\mathcal{A}$ of that isopycnal layer

$$\mathscr{J}_z^F = \iint_{\mathcal{A}} \nabla_h b \times \mathbf{F} \cdot \hat{k}\big|_{z=0} \mathrm{d}y\mathrm{d}x, \qquad (14)$$

An example of the geometry and outcrop area of the isopycnal layer used in the calculation is shown in Figure 7($a$). As shown in the figure, the regions of low PV are associated with anticyclonic circulations. The eddy PV flux (13) is positive over the latitudinal extent of the anticyclonic circulations, peaking near their centers (Figure 7($c$)). The full timeseries and meridional structure of the eddy PV flux is plotted as a Hovmöller diagram in Figure 8. Also plotted in the figure is the thickness weighted, isopycnally averaged PV. Similar to the instant shown in Figure 7($b$)-($c$), the maximum in the eddy PV flux tends to occur near the minimum in the mean PV, and propagates into the interior of the fluid as the low PV water is subducted. The maximum in the eddy PV flux, $\mathscr{J}_y^e\big|_{y=y_{max}}$, grows after the

[2]Note that this differs from the experiment described in *Thomas* [2007] where the zonal wind-stress was turned off midway through the run.

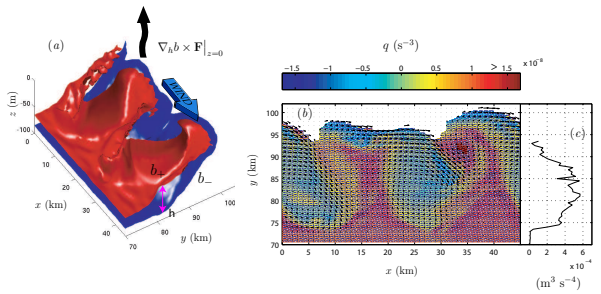


**Figure 7.** Frontal meandering and upward, along isopycnal eddy PV flux at the front with the eastward jet in the constant wind-stress experiment at $t = 5.6$ inertial periods after the onset of the winds. $(a)$ Upper (red) and lower (blue) isopycnal surfaces of density 28.3 and 28.5 kg m$^{-3}$, respectively, that bound the isopycnal layer used to calculated the net eddy and frictional PV fluxes. $(b)$ Isopycnal map of the PV (shades) and velocity (vectors) averaged in the vertical over the isopycnal layer shown in $(a)$. $(c)$ The correlation of the velocity and PV fields results in a net positive meridional eddy PV flux along the isopycnal layer $\iint q''v''\mathrm{d}z\mathrm{d}x > 0$.

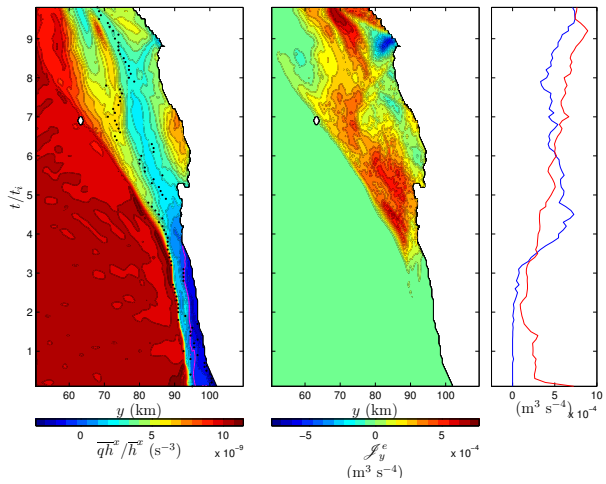


**Figure 8.** Hovmöller diagrams of (left) the thickness-weighted, mean PV and (middle) the net eddy PV flux $\mathscr{J}_y^e$ on the isopycnal layer shown in figure 7$(a)$. The location of the maximum eddy PV flux (dots) and the zero PV contour (magenta) are also plotted with $\overline{qh}^x/\overline{h}^x$. Timeseries of the maximum net eddy PV flux, $\mathscr{J}_y^e\big|_{y=y_{max}}$, (blue) and the frictional PV flux integrated over the outcrop area (red), $\mathscr{J}_z^F$, (right).

front goes unstable, peaking at $t \approx 4.5$ inertial periods, then levels out at a quasi-steady value close to the net frictional PV flux $\mathscr{J}_z^F$. Also note that for times before the onset of frontal instabilities, the lowest value of the mean PV is negative, however once the instabilities reach finite amplitude, the minimum in $\overline{qh}^x/\overline{h}^x$ switches to being positive. These results suggest that the eddy PV flux at fully three-dimensional wind-forced fronts scales with the surface frictional PV flux and that the PV pump mechanism holds in three-dimensions and limits the extreme low value of the PV to values greater than zero.

In the first of the two three-dimensional experiments, the wind was held constant so that the net frictional PV flux was always outward, and PV was constantly being extracted from the fluid. In the second experiment with a rotating wind vector (12), the frictional PV flux oscillates, both inputing and extracting PV in one cycle. Therefore one might expect that averaged over the period of rotation of the wind vector, the wind-stress would have no net effect on a fluid parcel's PV. This is true at the beginning of the experiment when the front is two-dimensional. During this stage, when the wind is upfront, Ekman flow advects lighter water over dense, stratifying the fluid and increasing the PV. Then, as the wind-turns downfront, that light water is pushed back to the less dense side of the front, the stratification is reduced and the PV returns to close to its initial value. Once the front goes unstable however, the process is no longer so reversible. A sequence of images of isopycnal maps of the PV is used to explain why this is so. After the formation of frontal meanders and following a period of down-front winds, low PV surface water is subducted into the interior where it is isolated from the Ekman layer and PV input during upfront winds (Figure 9 $(a)$-$(b)$). By leaving the frictional boundary layer in a time less than $T$, fluid parcels experience a net change in PV over a cycle. As the wind vector rotates to the upfront orientation, high PV is formed on the northern edge of the isopycnal outcrop (Figure 9 $(a)$-$(c)$). The high PV fluid subsequently collects into a surface intensified cyclone that pairs with a subsurface anticyclone associated with subducted low PV water, forming a propagating dipole vortex (Figure 9 $(c)$-$(f)$). The outcrop area of the cyclone forms a closed loop in contrast to the outcrop of the front that extends across the domain in the zonal direction. Consequently, the net frictional PV flux through the outcrop of the cyclone is zero regardless of the orientation of the wind, allowing the high PV in the cyclone to persist through periods of down-front winds.

As with the solution from the first experiment, the net eddy PV flux (13) was calculated and compared to the net frictional PV flux and structure of the thickness

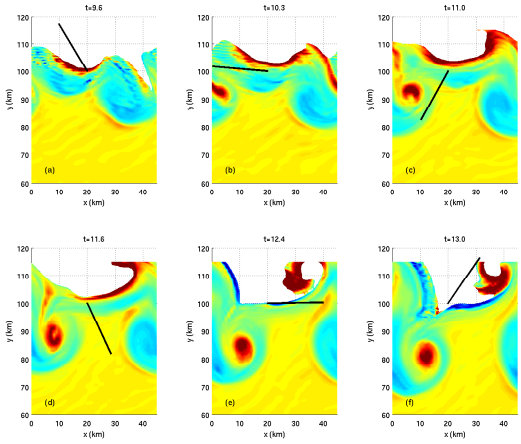


**Figure 9.** Temporal evolution of the PV on the 28.4 kg m$^{-3}$ isopycnal surface for the experiment with the rotating wind-vector. The black line denotes the orientation of the wind-stress and the time in inertial periods is indicated at the top of each panel.

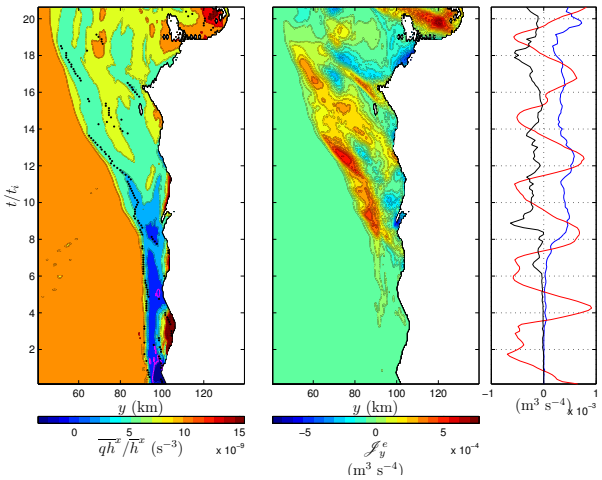


**Figure 10.** Hovmöller diagrams of (left) the thickness-weighted, mean PV and (middle) the net eddy PV flux $\mathcal{J}_y^e$ on the isopycnal layer bounded by the 28.3 and 28.5 kg m$^{-3}$ isopycnals for the experiment with the rotating wind-vector. The location of the maximum eddy PV flux (dots) and the zero PV contour (magenta) are also plotted with $\overline{qh}^x/\overline{h}^x$. Timeseries of the maximum (blue) and minimum (black) net eddy PV flux along with the the frictional PV flux integrated over the outcrop area (red), $\mathcal{J}_z^F$, (right).

weighted, mean PV (Figure 10). Similar to the constant wind-stress experiment, an upward eddy PV flux is associated with the subducting low PV water mass.

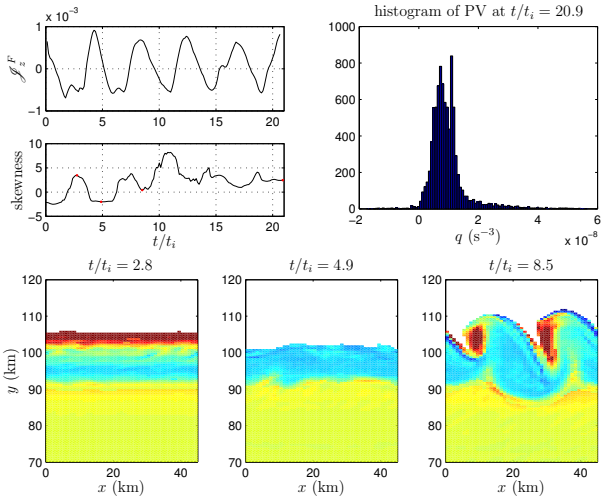


**Figure 11.** Upper left: timeseries of the net frictional PV flux and skewness of the PV distribution on the 28.4 kg m$^{-3}$ isopycnal surface for the rotating wind-vector experiment. Upper right: histogram of the PV on the 28.4 kg m$^{-3}$ isopycnal layer at $t = 20.9$ inertial periods. Bottom: PV field on the 28.4 kg m$^{-3}$ isopycnal surface at $t = 2.8$ and 4.9 inertial periods, when the front is two-dimensional, and at $t = 8.5$ inertial periods during the onset of instabilities.

There are also regions where $\mathcal{J}_y^e$ is negative. Timeseries of the maximum and minimum net eddy PV flux are compared to the integrated frictional PV flux in Figure 10($c$). As can be seen in the figure, $\mathcal{J}_z^F$ oscillates with the three day period of the wind while the maximum and minimum eddy PV flux intensifies once the front goes unstable and then saturates. The value that the extrema in the eddy PV flux take after saturation approach the maximum and minimum values of the frictional PV flux. Looking at the structure of $\mathcal{J}_y^e$ in detail, during times near the maximum in $\mathcal{J}_z^F$, an upward eddy PV flux develops at the surface and propagates into the interior (e.g. $t = 8, 12, 16$ inertial periods). The matching of the frictional and eddy PV fluxes suggests that the PV pump mechanism is active with a time-dependent wind-stress and that the submesoscale eddies responsible for the advective PV flux can respond to relatively fast changes in the wind-stress.

Another signature of the PV pump mechanism is the limitation of the minimum PV to values greater than zero. This is also seen in the rotating wind experiment as the thickness weighted mean PV is positive at all locations after the front goes unstable. The effect of the frontal instabilities on the extrema in the PV is most clearly illustrated by examining distributions of the PV on isopycnals. Histograms of the PV calculated on the

isopycnal outcropping at the front taken near the end of the experiment is characterized by a long tail for $q > 0$ and a rapid decrease near $q = 0$, causing the PV distribution to have positive skewness (Figure 11). Time-series of the skewness and net frictional PV flux reveal that before the onset of frontal instabilities, the skewness oscillates nearly in quadrature with $\mathscr{J}_z^F$. This is the time period when the front and the PV field remains two-dimensional and, as mentioned previously, there is the near reversible change in PV. Once the instabilities grow to finite amplitude however, the skewness remains positive, indicating the effectiveness of the PV pump mechanism to limit the extreme low values of the PV.

## Conclusions

When a baroclinic current is forced by a down-front wind, an upward frictional PV flux is induced that extracts PV from the fluid and destabilizes the flow. Instabilities ensue that act as a PV pump, drawing high PV from the pycnocline while subducting low PV from the surface via an eddy PV flux proportional to the frictional PV flux. This mechanism tends to keep the extreme low value of the PV from dropping below zero at the expense of reducing the PV in the interior of the fluid. When the current is forced by a wind that alternates in orientation, and hence alternately supplies and removes PV, the PV pump mechanism limits the reduction of PV during periods of down-front winds but not the injection of PV by up-front winds. This causes the skewness of the isopycnal PV distribution to become positive.

The limitation of the extreme minima in the PV to values near zero has also been observed in numerical simulations of baroclinic flows forced by atmospheric buoyancy loss (e.g. *Haine and Marshall* [1998], *Legg et al.* [1998], and *Straneo et al.* [2002]). In such simulations, in contrast to the experiments presented here, the PV flux at the surface is provided by diabatic processes and not by frictional forces. In spite of their different forcing mechanisms, the similarities in the PV distributions seen in both types of simulations suggests that an analagous PV pump mechanism involving eddy and surface diabatic PV fluxes may be active at buoyancy forced baroclinic currents. It would be of interest to see if there is a general relation between eddy and surface frictional and diabatic PV fluxes because it would imply that a parameterization for eddy PV fluxes in the upper ocean should take into account atmospheric forcing.

**Acknowledgments.** I would like to thank Chris Garrett and Peter Müller for their invitation to the Aha Hulikoa workshop. This research was supported by NSF grants OCE-0549699 and OCE-0612058.

## References

Boccaletti, G., R. Ferrari, and B. Fox-Kemper, Mixed layer instabilities and restratification, *J. Phys. Oceanogr.*, 2007, in press.

Haine, T. W. N., and J. Marshall, Gravitational, symmetric, and baroclinic instability of the ocean mixed layer, *J. Phys. Oceanogr.*, *28*, 634–658, 1998.

Hoskins, B. J., The role of potential vorticity in symmetric stability and instability, *Qt. J. R. Met. Soc.*, *100*, 480–482, 1974.

Hoskins, B. J., M. E. McIntyre, and A. W. Robertson, On the use and significance of isentropic potential vorticity maps, *Qt. J. R. Met. Soc.*, *111*, 877–946, 1985.

Hua, B., D. W. Moore, and S. L. Gentil, Inertial nonlinear equilibration of equatorial flows, *J. Fluid Mech.*, *331*, 345–371, 1997.

Legg, S., J. McWilliams, and J. Gao, Localization of deep convection by a mesoscale eddy, *J. Phys. Oceanogr.*, *28*, 944–970, 1998.

Marshall, J. C., and A. J. G. Nurser, Fluid dynamics of oceanic thermocline ventilation., *J. Phys. Oceanogr.*, *22*, 583–595, 1992.

McWilliams, J. C., I. Yavneh, M. J. P. Cullen, and P. R. Gent, The breakdown of large-scale flows in rotating, stratified fluids, *Phys. Fluids*, *10*, 3178–3184, 1998.

Richards, K. J., and N. R. Edwards, Lateral mixing in the equatorial Pacific: The importance of inertial instability, *Geophys. Res. Lett.*, *30*, 2003, doi:10.1029/2003GL017768.

Shchepetkin, A. F., and J. C. McWilliams, The Regional Ocean Modeling System (ROMS): a split-explicit, free-surface, topography-following coordinate oceanic model., *Ocean Modelling*, 2004, in press.

Straneo, F., M. Kawase, and S. Riser, Idealized models of slantwise convection in a baroclinic flow, *J. Phys. Oceanogr.*, *32*, 558–572, 2002.

Thomas, L. N., Destruction of potential vorticity by winds, *J. Phys. Oceanogr.*, *35*, 2005.

Thomas, L. N., Formation of intrathermocline eddies at ocean fronts by wind-driven destruction of potential vorticity, *Dyn. Atmos. Oceans*, 2007, accepted.

Thomas, L. N., and R. Ferrari, Friction, frontogenesis, frontal instabilities and the stratification of the surface mixed layer, *J. Phys. Oceanogr.*, 2007, submitted.

Thomas, L. N., and C. M. Lee, Intensification of ocean fronts by down-front winds, *J. Phys. Oceanogr.*, *35*, 1086–1102, 2005.

Thorpe, A. J., and R. Rotunno, Nonlinear aspects of symmetric instability, *J. Atmos. Sci.*, *46*, 1285–1299, 1989.

This preprint was prepared with AGU's LaTeX macros v4, with the extension package 'AGU$^{++}$' by P. W. Daly, version 1.6a from 1999/05/21.